Check for updates

How to cite: *Angew. Chem. Int. Ed.* **2021**, *60*, 11201–11205
International Edition: doi.org/10.1002/anie.202100942
German Edition: doi.org/10.1002/ange.202100942

Supramolecular Chemistry

Chemical Reduction of a Nanosized [6]Cyclo-2,7-naphthylene Macrocycle

Zheng Zhou, Zheng Wei, Koki Ikemoto, Sota Sato, Hiroyuki Isobe, and Marina A. Petrukhina**

Abstract: *Chemical reduction of a naphthylene macrocycle, [6]cyclo-2,7-naphthylene ([6]CNAP, **1**), with alkali metals, Li and K, revealed the accessibility of the doubly-reduced state of **1**. The macrocyclic $\mathbf{1}^{2-}$ anion was isolated in different coordination environments and crystallographically characterized. The single-crystal X-ray diffraction confirmed the formation of contact-ion complexes with one Li^+ and two K^+ ions in THF, and a "naked" dianion in the solvent-separated ion product with K^+ ions in the presence of 18-crown-6 ether. The detailed structural analysis of $\mathbf{1}^{2-}$ showed that the π-conjugation over the biaryl linkages between naphthylene panels were enhanced upon two-fold reduction, which was rationally explained by theoretical calculations.*

Redox properties of the smallest acene, naphthalene, have played an important role in chemistry and materials science. For instance, alkali-metal naphthalenides have been widely used in organic synthesis as useful reductants.[1] The redox behavior of the naphthalene was also a determinant factor to enable the first non-ohmic charge carrier transport in organic materials.[2] In-depth understanding of the outcomes of reduction has been derived by the precise structural information from crystallographic analyses.[3] The recent improvement of synthetic methods has allowed the preparation of carbon-rich polycyclic aromatic hydrocarbons (PAHs) with topological variations, including negative or positive curvatures,[4] partial defects,[5] and fragment-hybridizations.[6] These novel molecular nanocarbons exhibit remarkable performance in energy storage materials,[7] semiconductors,[8] and optoelectrical devices[9] owing to their outstanding chemical and physical properties. Moreover, charging non-planar PAHs with electrons along with investigation of their electronic and structural responses[10] showed that redox processes are topology- and charge-dependent. Extensive X-ray diffraction studies of electron transfer for carbon bowls,[11] belts,[12] wires,[13] and helicenes[14] revealed unusual reactivity, unique metal binding and remarkable supramolecular assembly patterns of the negatively charged π-systems, thus prompting a broad exploration of novel curved nanocarbon frameworks.

Recently, simple and concise transformations of naphthalene opened novel possibilities in modern electronics applications. A hexagonal macrocycle, [6]cyclo-2,7-naphthylene ([6]CNAP), worked as a bipolar transport material in organic light-emitting devices[15] and as a spin valve in spintronics devices[16] through its rich redox behavior. In addition, mediated by its complexation with alkali-metals, [6]CNAP functioned as a high-capacity, negative electrode material in an all-solid-state lithium rechargeable battery, which surpassed the capacity of conventional graphite electrodes.[7b] However, structural information of the naphthylene macrocycles at the redox states has been scarce, and crystal structures of the reduced products have never been disclosed, including other cyclonaphthylene congeners that were synthesized after [6]CNAP.[17] We herein present the first study of the chemical reduction behavior of a naphthylene macrocycle with Li and K metals along with the crystallographic report of its doubly-reduced products.

The crystal structure of solvent-free [6]CNAP ($C_{60}H_{36}$, **1**) was reported back in 2011 using crystallization from anthracene melt (**1-a**).[15,18] In 2016, a solvent-containing polymorph, $C_{60}H_{36}{\cdot}C_6H_4Cl_2$ (**1-b**), was reported.[7b] The inclusion of dichlorobenzene molecule shows the potential of **1** for internal guest entrapment, which is commonly seen in various cycloparaphenylenes (CPPs).[19] In this work, gas-phase sublimation at 500 °C used for purification of **1** afforded colorless plates in ca. 40 % yield. The X-ray diffraction characterization reveals that this high-temperature solvent-free polymorph (**1-c**) belongs to a different space group than **1-a** (*See Supporting Information for more details*),[20] although their volumes per molecule (961 vs. 966 Å^3, respectively) are comparable.

Despite the axial twists between the naphthylene panels, the macrocyclic ring of **1** has a more planarized core (Figure 1) compared with [8]CPP that has a close d_R (Figure S11). This can be illustrated by the dihedral angles (ω) between the naphthylene units and the central plane R that are much smaller in **1-c** (avg. 18.5° vs. 74.8° in [8]CPP[12c]). As a result, the measured volume of the internal cavity in **1-c** (ca. 291 Å^3) is more comparable to the smaller [6]CPP[12c] (233 Å^3).

In the crystal structure of **1-c**, the molecules are arranged in a herringbone pattern similar to **1-a** forming a 2D layer through both π···π (3.114(7)-3.198(7) Å) and C–H···π (2.681-(7)-2.703(7) Å) interactions (Figure S12). The internal space of the macrocycle is occupied by the naphthylene units from two adjacent molecules (Figure S13), thus preventing formation of a porous structure.

[*] Dr. Z. Zhou, Dr. Z. Wei, Prof. Dr. M. A. Petrukhina
Department of Chemistry
University at Albany, State University of New York
1400 Washington Ave, Albany, NY 12222 (USA)
E-mail: mpetrukhina@albany.edu
Dr. K. Ikemoto, Dr. S. Sato, Prof. Dr. H. Isobe
Department of Chemistry
The University of Tokyo
Hongo 7-3-1, Bunkyo-ku, Tokyo, 113-0033 (Japan)
E-mail: isobe@chem.s.u-tokyo.ac.jp
Supporting information and the ORCID identification number(s) for the author(s) of this article can be found under: https://doi.org/10.1002/anie.202100942.

 © 2021 Wiley-VCH GmbH

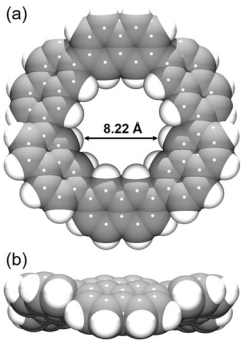

Figure 1. a) Face and b) side views of **1-c**, space-filling models.[20]

The chemical reduction of **1** with Li metal in THF at room temperature proceeds through two distinctive steps, as detected by UV/Vis spectroscopy (Figure S1). The reaction solution quickly turns to a deep green color, which is indicative of the doubly reduced state $\mathbf{1}^{2-}$ (Figures S2–S6). By slow diffusion of hexanes, the dianion was successfully crystallized with two lithium counterions as dark green plates in moderate yield (57%). The X-ray diffraction analysis confirmed the formation of the contact-ion complex, $[Li^+(THF)_4][\{Li^+(THF)_3\}(\mathbf{1}^{2-})]\cdot THF$ (**2**). When the reduction was performed with K metal in the presence of 18-crown-6, a solvent-separated ion product was obtained in good yield (75%) and crystallographically characterized as $[\{K^+(18\text{-crown-6})(THF)_2\}_2](\mathbf{1}^{2-})\cdot 4THF$ (**3**). In the absence of 18-crown-6, the K-induced reduction of **1** afforded the contact-ion complex, $[\{K^+(THF)_4\}_2(\mathbf{1}^{2-})]\cdot THF$ (**4**) (Scheme 1, see Supporting Information for more details).

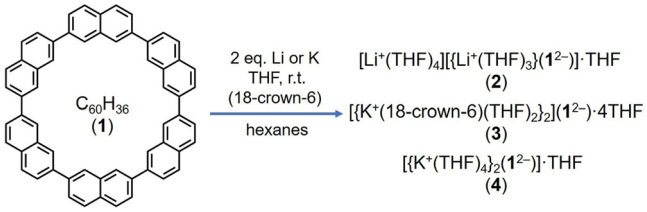

Scheme 1. Chemical reduction of **1** with Li and K metals.

In the crystal structure of **2** (Figure 2a), there are two independent Li^+ ions along with a doubly-reduced anion, $\mathbf{1}^{2-}$.[20] The Li1 ion is bound to one benzene ring of $\mathbf{1}^{2-}$ in an asymmetric fashion with two short Li···C distances of 2.573(30) Å and 2.772(30) Å and four much longer contacts (2.983(30)-3.430(30) Å, Figure 2c). The coordination of Li1 ion is completed by three THF molecules with the Li···O_{THF} distances of 1.917(30)-2.002(30) Å. The Li2 ion is wrapped by four THF molecules (Li···O_{THF}: 1.882(30)-2.069(30) Å), allowing the $[Li^+(THF)_4]$ moiety to be solvent-separated from the monoanionic $[\{Li^+(THF)_3\}(\mathbf{1}^{2-})]^-$ complex. All Li···C and Li···O distances are close to those previously reported.[11a] Notably, the internal space of $\mathbf{1}^{2-}$ (ca. 322 Å^3) is occupied by one interstitial THF molecule (Figure 2b).

In the crystal structure of **3** (Figure 3), two independent $\{K^+(18\text{-crown-6})(THF)_2\}$ moieties are solvent-separated from

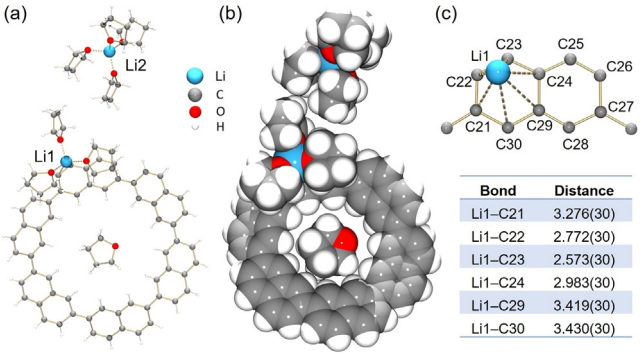

Bond	Distance
Li1–C21	3.276(30)
Li1–C22	2.772(30)
Li1–C23	2.573(30)
Li1–C24	2.983(30)
Li1–C29	3.419(30)
Li1–C30	3.430(30)

Figure 2. Crystal structure of **2**, a) ball-and-stick and b) space-filling models, c) metal coordination along with a table of Li–C distances.[20]

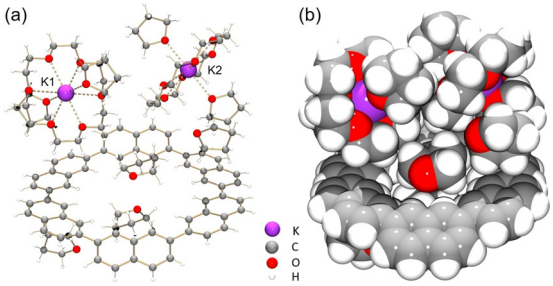

Figure 3. Crystal structure of **3**, a) ball-and-stick and b) space-filling models.[20]

$\mathbf{1}^{2-}$, providing a unique example of the "naked" dianion that allows the evaluation of its core deformation upon reduction without metal binding influence.[20] Each K^+ ion is equatorially bound to an 18-crown-6 ether molecule (K··O_{crown}: 2.776(3)-2.896(3) Å) and axially coordinated to two THF molecules (K··O_{THF}: 2.653(6)-2.731(6) Å), with all values being close to those previously reported.[14] The internal void of the $\mathbf{1}^{2-}$ macrocycle ($V_{void} \approx 290$ Å^3, Figure S11) is filled by two interstitial THF molecules (Figure 3b). Two additional THF molecules occupy the cavities in the crystal structure without notable interactions.

In contrast to **3**, two independent K^+ ions are externally coordinated to the doubly-reduced macrocycle in the crystal structure of **4** (Figure 4).[20] The K1 ion is bound to one ring of the naphthylene unit (C) in a η^5-mode with the corresponding K··C distances of 3.136(6)-3.274(6) Å (Figure 4c). The K2 ion binds to the ring F on the opposite side in a η^4-mode with the K··C distances of 2.992(6)-3.367(6) Å.[3c,12a] The coordination of each K^+ ion is completed by four THF molecules, with the K··O_{THF} distances of 2.583(6)-2.744(6) Å and 2.628(6)-2.997(6) Å.[10b,12a,b] Similar to **2**, only one interstitial THF molecule is encapsulated inside the internal void of $\mathbf{1}^{2-}$ ($V_{void} \approx 296$ Å^3) in **4** (Figure 4b).

Interestingly, no metal ion encapsulation inside the internal cavity of $\mathbf{1}^{2-}$ is seen in **2**–**4** in contrast to the CPP family.[12a] For example, the internal volume of the $[8]CPP^{2-}$ anion is increased by ca. 100 Å^3 in comparison to its neutral state, allowing accommodation of large $\{K^+(18\text{-crown-6})\}$ moieties.[12c] In contrast, the internal volume of the $\mathbf{1}^{2-}$

 © 2021 Wiley-VCH GmbH

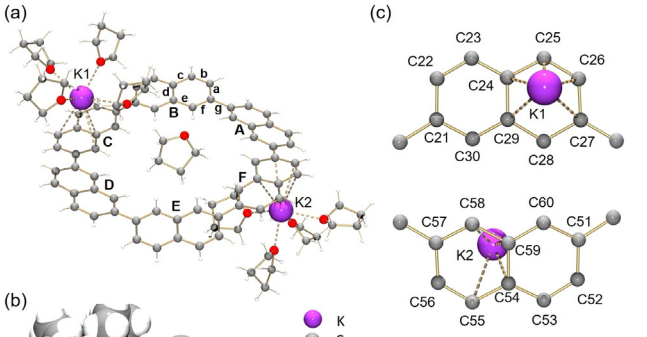

Bond	Distance	Bond	Distance
K1–C24	3.136(6)	K2–C54	2.992(6)
K1–C25	3.163(6)	K2–C55	3.288(6)
K1–C26	3.147(6)	K2–C56	3.524(6)
K1–C27	3.274(6)	K2–C57	3.565(6)
K1–C28	3.539(8)	K2–C58	3.367(7)
K1–C29	3.202(5)	K2–C59	3.005(6)

Figure 4. Crystal structure of **4**, a) ball-and-stick and b) space-filling models, c) metal coordination along with a table of K–C distances.[20]

macrocycle remains almost unchanged (aver. 303 vs. 291 Å^3 in **1-c**), with the core geometry being less affected by electron transfer.

Products **3** and **4** provide a very good pair for evaluation of the macrocyclic core deformation upon two-fold reduction without metal binding (**3**) and with two coordinated metal ions (**4**). The aromaticity changes of naphthylene units in $\mathbf{1}^{2-}$ were analyzed by comparing the C–C bond length distances and core planarity in **3** and **4** with those in **1-c**. In **3**, the C–C bonds of $\mathbf{1}^{2-}$ at **e** and **f** positions are slightly elongated, but other bonds remain unchanged compared to the neutral state (Table 1). Due to direct metal coordination in **4**, the C–C

Table 1: Average bond length distances (Å) in **1-c** and $\mathbf{1}^{2-}$ in **3** and **4**.

	1-c	1^{2-} (3)	1^{2-} (units A, B, D, E) (4)	1^{2-} (units C, F) (4)
a	1.425(7)	1.417(7)	1.422(8)	1.410(8)
b	1.365(7)	1.372(7)	1.363(8)	1.379(8)
c	1.414(7)	1.414(7)	1.410(8)	1.411(8)
d	1.415(7)	1.426(7)	1.421(8)	1.438(8)
e	1.408(7)	1.418(7)	1.408(8)	1.429(8)
f	1.381(7)	1.402(7)	1.391(8)	1.427(8)
g	1.479(7)	1.471(7)	1.476(8)	1.432(8)

bonds at **b**, **d**, and **f** sites in units C and F of $\mathbf{1}^{2-}$ are elongated in comparison with those in uncomplexed sites. Meanwhile, the C–C bonds at **g** sites near units C and F are much shorter than those in other units (1.432(8) Å and 1.476(8) Å, respectively). According to the planarity calculations, the average distance from the weighted least-square plane of 0.020 Å in **1-c** is increased to 0.031 Å in $\mathbf{1}^{2-}$ (**3**), indicating that naphthylene panels become slightly curved in the "naked" dianion (Tables S5 and S7). In $\mathbf{1}^{2-}$ (**4**), the units A, B, D, and E remain planar (RMSD/A: 0.012 Å, Table S8), while units C and F affected by direct metal coordination show deviation from planarity (RMSD/A: 0.123 Å and 0.074 Å, respectively).

The geometry changes upon chemical reduction and metal binding detected for the [6]CNAP macrocycle by evaluation of bending and dihedral angles (Figure 5) are two-fold. On one hand, the whole macrocycle core becomes more planar when charged with two electrons, and this effect is less symmetric in $\mathbf{1}^{2-}$ (**3**) due to the single Li^+ ion coordination (Figure 5c, Table S3). On the other hand, an increase in bending of the naphthylene units is found going from **1-c** to $\mathbf{1}^{2-}$ (**4**), and this change is especially noticeable for units C and F directly engaged in coordination (Figure 5b, Table S2).

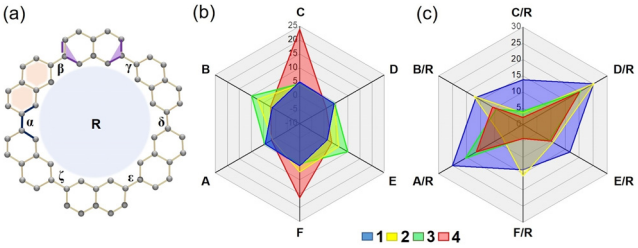

Figure 5. a) Calculation of bending (purple) and dihedral (orange) angles (°) in **1-c** and $\mathbf{1}^{2-}$ in **2**–**4**, and b,c) their visualized comparison.

The solid-state structures of **2**–**4** exhibit the herringbone packing of complementary cationic and anionic counterparts (Figure 6). The angle between the macrocycles in the adjacent columns is increased from 47.6° in **1-c** to 74.6° in **3**, 79.6° in **2**, and 88.6° in **4** (Figure S15). This is accompanied by an increase of the calculated volume per "molecule" along the series: from 961 Å^3 in **1-c** to 1990 Å^3 in **2**, 2624 Å^3 in **3**, and 1969 Å^3 in **4**. In all cases the 2D layered structures are formed through C–H···π interactions between the $\mathbf{1}^{2-}$ anions and the adjacent cationic moieties (Figures S16–S18).

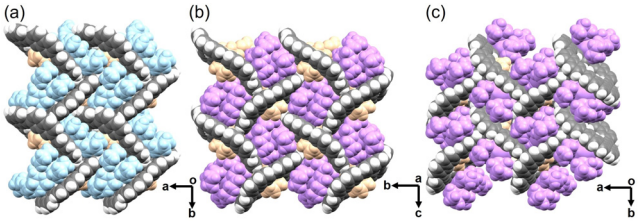

Figure 6. Solid-state structures in a) **2**, b) **3**, and c) **4**.

Structural changes associated with the two-electron reduction were further analyzed by theoretical calculations. We obtained theoretical structures of neutral **1** and dianion $\mathbf{1}^{2-}$ by using density functional theory (DFT) at the B3LYP level of theory with the 6-31G(d,p) basis set.[21] As shown in Figure 7, the DFT calculations qualitatively reproduced the structural changes at the biaryl linkages. The dihedral angle estimated as 35° in **1** was reduced to 23° upon two-fold reduction in $\mathbf{1}^{2-}$. This tendency was experimentally observed in the above crystal structures. When the origin of this structural change was investigated with anisotropy of the current induced density (ACID) analyses,[22] extensions of the π-conjugation through the nanosized macrocycle were indi-

 © 2021 Wiley-VCH GmbH

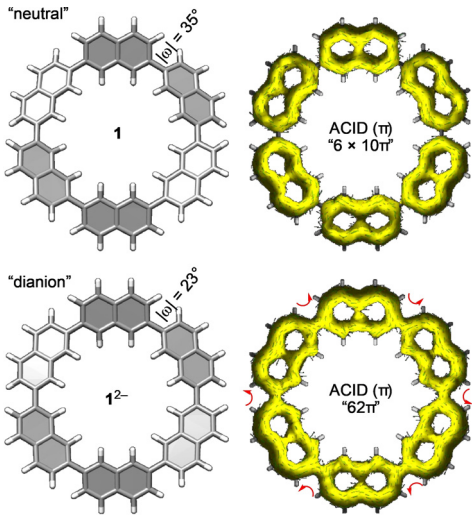

Figure 7. The calculated structures and ACID surfaces of **1** and $\mathbf{1}^{2-}$.

cated as the origin. Thus, the ACID (π) surfaces of neutral **1** expectedly showed the presence of 6 aromatic panels comprising 10π naphthylene systems ("$6\times10\pi$"; Figures 7, S19, S20), whereas the biaryl linkages of $\mathbf{1}^{2-}$ were covered with the ACID (π) surfaces, showing the presence of large 62π conjugated system.

Thus, the extended π-conjugation over the biaryl linkages should be the origin of the ω reduction upon two-electron acquisition, which also resulted in the emergence of global aromaticity over the macrocyclic [6]CNAP structure.[23]

In summary, chemical reduction of [6]CNAP (**1**) macrocycle with Li and K metals provided ready access to its doubly-reduced state, $\mathbf{1}^{2-}$, which was crystallized in different coordination environments. The use of different alkali metals allowed the formation of two contact-ion products (CIP), with one or two metal ions externally coordinated to the $\mathbf{1}^{2-}$ core. The addition of secondary coordinating agent, 18-crown-6 ether, enabled switching the metal binding off in a solvent-separated-ion product (SSIP). The direct comparison of the "naked" and complexed forms of $\mathbf{1}^{2-}$ with neutral parent disentangled structural deformation of the macrocyclic core upon two-electron reduction in SSIP from additional metal binding effects observed in CIP with two K^+ ions. The detected macrocycle core planarization and small internal volume of $\mathbf{1}^{2-}$ could be the reason for the entrapment of only THF molecules inside the central void seen in all crystalline products. Importantly, this study showed that the π-extension as well as global aromaticity may be the unique origin of favorable redox behavior of [6]CNAP as the effective electrode materials.[7]

Acknowledgements

Finacial support of this work from the U.S. National Science Foundation, CHE-2003411, is gratefully acknowledged by M.A.P. NSF's ChemMatCARS Sector 15 is principally supported by the Divisions of Chemistry (CHE) and Materials Research (DMR), National Science Foundation, under grant number NSF/CHE-1346572. Use of the Advanced Photon Source, an Office of Science User Facility operated for the U.S. Department of Energy (DOE) Office of Science by Argonne National Laboratory, was supported by the U.S. DOE under Contract No. DE-AC02-06CH11357. The authors also thank JSPS KAKENHI (20H05672, 20K15254, 19K22180, 19H02552) for financial support.

Conflict of interest

The authors declare no conflict of interest.

Keywords: alkali metals · chemical reduction · macrocycles · structural study · X-ray diffraction

[1] K. M. Short in *Encyclopedia of Reagents for Organic Synthesis*, *Vol. 5* (Ed.: L. Paquett), Wiley, Chichester, **1995**, pp. 3151 – 3153.
[2] N. Karl, *Synth. Met.* **2003**, *133*, 649 – 657.
[3] a) J. J. Brooks, W. Rhine, G. D. Stucky, *J. Am. Chem. Soc.* **1972**, *94*, 7346 – 7351; b) C. Melero, A. Guijarro, M. Yus, *Dalton Trans.* **2009**, 1286 – 1289; c) T. A. Scott, B. A. Ooro, D. J. Collins, M. Shatruk, A. Yakovenko, K. R. Dunbar, H.-C. Zhou, *Chem. Commun.* **2009**, 65 – 67.
[4] a) M. Ball, Y. Zhong, Y. Wu, C. Schenck, F. Ng, M. Steigerwald, S. Xiao, C. Nuckolls, *Acc. Chem. Res.* **2015**, *48*, 267 – 276; b) S. H. Pun, Q. Miao, *Acc. Chem. Res.* **2018**, *51*, 1630 – 1642; c) Y. Segawa, D. R. Levine, K. Itami, *Acc. Chem. Res.* **2019**, *52*, 2760 – 2767.
[5] a) I. V. Alabugin, E. Gonzalez-Rodriguez, *Acc. Chem. Res.* **2018**, *51*, 1206 – 1219; b) Z. Sun, K. Ikemoto, T. M. Fukunaga, T. Koretsune, R. Arita, S. Sato, H. Isobe, *Science* **2019**, *363*, 151 – 155.
[6] a) K. Kawasumi, Q. Zhang, Y. Segawa, L. T. Scott, K. Itami, *Nat. Chem.* **2013**, *5*, 739 – 744; b) J. M. Fernández-García, P. J. Evans, S. Filippone, M. Á. Herranz, N. Martín, *Acc. Chem. Res.* **2019**, *52*, 1565 – 1574.
[7] a) D. Odkhuu, D. Jung, H. Lee, S. S. Han, S.-H. Choi, R. Ruoff, N. Park, *Carbon* **2014**, *66*, 39 – 47; b) S. Sato, A. Unemoto, T. Ikeda, S.-i. Orimo, H. Isobe, *Small* **2016**, *12*, 3381 – 3387.
[8] a) X. Lin, B. Wegner, K. M. Lee, M. A. Fusella, F. Zhang, K. Moudgil, B. P. Rand, S. Barlow, S. R. Marder, N. Koch, A. Kahn, *Nat. Mater.* **2017**, *16*, 1209 – 1215; b) A. Narita, Z. Chen, Q. Chen, K. Müllen, *Chem. Sci.* **2019**, *10*, 964 – 975.
[9] a) B. Zhang, M. T. Trinh, B. Fowler, M. Ball, Q. Xu, F. Ng, M. L. Steigerwald, X. Y. Zhu, C. Nuckolls, Y. Zhong, *J. Am. Chem. Soc.* **2016**, *138*, 16426 – 16431; b) A. M. Rice, W. B. Fellows, E. A. Dolgopolova, A. B. Greytak, A. K. Vannucci, M. D. Smith, S. G. Karakalos, J. A. Krause, S. M. Avdoshenko, A. A. Popov, N. B. Shustova, *Angew. Chem. Int. Ed.* **2017**, *56*, 4525 – 4529; *Angew. Chem.* **2017**, *129*, 4596 – 4600.
[10] a) R. Benshafrut, E. Shabtai, M. Rabinovitz, L. T. Scott, *Eur. J. Org. Chem.* **2000**, 1091 – 1106; b) A. V. Zabula, S. N. Spisak, A. S. Filatov, A. Yu. Rogachev, M. A. Petrukhina, *Acc. Chem. Res.* **2018**, *51*, 1541 – 1549; c) M. A. Petrukhina, *Dalton Trans.* **2019**, *48*, 5125 – 5130.
[11] a) A. V. Zabula, A. S. Filatov, S. N. Spisak, A. Yu. Rogachev, M. A. Petrukhina, *Science* **2011**, *333*, 1008 – 1011; b) S. N. Spisak, Z. Wei, N. J. O'Neil, A. Yu. Rogachev, T. Amaya, T. Hirao, M. A. Petrukhina, *J. Am. Chem. Soc.* **2015**, *137*, 9768 – 9771; c) A. V. Zabula, S. N. Spisak, A. S. Filatov, A. Yu. Rogachev, R. Clérac, M. A. Petrukhina, *Chem. Sci.* **2016**, *7*, 1954 – 1961; d) S. N. Spisak, Z. Wei, A. Yu. Rogachev, T. Amaya, T. Hirao, M. A. Petrukhina, *Angew. Chem. Int. Ed.* **2017**, *56*, 2582 – 2587;

 © 2021 Wiley-VCH GmbH

Angew. Chem. **2017**, *129*, 2626 – 2631; e) S. N. Spisak, A. Yu. Rogachev, A. V. Zabula, A. S. Filatov, R. Clérac, M. A. Petrukhina, *Chem. Sci.* **2017**, *8*, 3137 – 3145.

[12] a) A. V. Zabula, A. S. Filatov, J. Xia, R. Jasti, M. A. Petrukhina, *Angew. Chem. Int. Ed.* **2013**, *52*, 5033 – 5036; *Angew. Chem.* **2013**, *125*, 5137 – 5140; b) S. N. Spisak, Z. Wei, E. Darzi, R. Jasti, M. A. Petrukhina, *Chem. Commun.* **2018**, *54*, 7818 – 7821; c) Z. Zhou, Z. Wei, T. A. Schaub, R. Jasti, M. A. Petrukhina, *Chem. Sci.* **2020**, *11*, 9305 – 9401.

[13] S. N. Spisak, M. U. Bühringer, Z. Wei, Z. Zhou, R. R. Tykwinski, M. A. Petrukhina, *Angew. Chem. Int. Ed.* **2019**, *58*, 2023 – 2028; *Angew. Chem.* **2019**, *131*, 2045 – 2050.

[14] a) Z. Zhou, X.-Y. Wang, Z. Wei, K. Müllen, M. A. Petrukhina, *Angew. Chem. Int. Ed.* **2019**, *58*, 14969 – 14973; *Angew. Chem.* **2019**, *131*, 15111 – 15115; b) Z. Zhou, R. K. Kawade, Z. Wei, F. Kuriakose, O. Ungor, M. Jo, M. Shatruk, R. Gershoni-Poranne, M. A. Petrukhina, I. V. Alabugin, *Angew. Chem. Int. Ed.* **2020**, *59*, 1256 – 1262; *Angew. Chem.* **2020**, *132*, 1272 – 1278; c) Z. Zhou, L. Fu, Y. Hu, X. Y. Wang, Z. Wei, A. Narita, K. Müllen, M. A. Petrukhina, *Angew. Chem. Int. Ed.* **2020**, *59*, 15923 – 15927.

[15] W. Nakanishi, T. Yoshioka, H. Taka, J. Y. Xue, H. Kita, H. Isobe, *Angew. Chem. Int. Ed.* **2011**, *50*, 5323 – 5326; *Angew. Chem.* **2011**, *123*, 5435 – 5438.

[16] K. Z. Suzuki, T. Izumi, X. M. Zhang, A. Sugihara, S. T. Pham, H. Taka, S. Sato, H. Isobe, S. Mizukami, *Appl. Mater.* **2017**, *5*, 046101.

[17] a) A. Yagi, Y. Segawa, K. Itami, *J. Am. Chem. Soc.* **2012**, *134*, 2962 – 2965; b) Z. Sun, P. Sarkar, T. Suenaga, S. Sato, H. Isobe, *Angew. Chem. Int. Ed.* **2015**, *54*, 12800 – 12804; *Angew. Chem.* **2015**, *127*, 12991 – 12995; c) Z. Sun, T. Suenaga, P. Sarkar, S. Sato, M. Kotani, H. Isobe, *Proc. Natl. Acad. Sci. USA* **2016**, *113*, 8109 – 8114.

[18] W. Nakanishi, J. Y. Xue, T. Yoshioka, H. Isobe, *Acta Crystallogr. Sect. E* **2011**, *67*, 1762 – 1763.

[19] a) J. Xia, J. W. Bacon, R. Jasti, *Chem. Sci.* **2012**, *3*, 3018 – 3021; b) H. Ueno, T. Nishihara, Y. Segawa, K. Itami, *Angew. Chem. Int. Ed.* **2015**, *54*, 3707 – 3711; *Angew. Chem.* **2015**, *127*, 3778 – 3782; c) N. Ozaki, H. Sakamoto, T. Nishihara, T. Fujimori, Y. Hijikata, R. Kimura, S. Irle, K. Itami, *Angew. Chem. Int. Ed.* **2017**, *56*, 11196 – 11202; *Angew. Chem.* **2017**, *129*, 11348 – 11354.

[20] Deposition numbers 2057092 (for **1-c**), 2057093 (for **2**), 2057094 (for **3**), and 2057095 (for **4**) contain the supplementary crystallographic data for this paper. These data are provided free of charge by the joint Cambridge Crystallographic Data Centre and Fachinformationszentrum Karlsruhe Access Structures service.

[21] a) A. D. Becke, *J. Chem. Phys.* **1993**, *98*, 5648 – 5652; b) A. D. Becke, *Phys. Rev. A* **1988**, *38*, 3098 – 3100; c) C. Lee, W. Yang, R. G. Parr, *Phys. Rev. B* **1988**, *37*, 785 – 789.

[22] D. Geuenich, K. Hess, F. Köhler, R. Herges, *Chem. Rev.* **2005**, *105*, 3758 – 3772.

[23] a) M. K. Cyrañski, T. M. Krygowski, M. Wisiorowski, N. J. R. van Eikema Hommes, P. v. R. Schleyer, *Angew. Chem. Int. Ed.* **1998**, *37*, 177 – 180; *Angew. Chem.* **1998**, *110*, 187 – 190; b) N. Toriumi, A. Muranaka, E. Kayahara, S. Yamago, M. Uchiyama, *J. Am. Chem. Soc.* **2015**, *137*, 82 – 85; c) M. D. Peeks, T. D. W. Claridge, H. L. Anderson, *Nature* **2017**, *541*, 200 – 203; d) C. Liu, M. E. Sandoval-Salinas, Y. Hong, T. Y. Gopalakrishna, H. Phan, N. Aratani, T. S. Herng, J. Ding, H. Yamada, D. Kim, D. Casanova, J. Wu, *Chem* **2018**, *4*, 1586 – 1595.

Manuscript received: January 20, 2021
Accepted manuscript online: February 22, 2021
Version of record online: April 8, 2021

 © 2021 Wiley-VCH GmbH